UNDERSTANDING THE SPATIAL DISTRIBUTION OF SNOW WATER EQUIVALENT IN PAIRED BASINS IN SOUTHWEST MONTANA, USA

Jason Welz[1], Jordy Hendrikx [1], Stuart Challender[2], and Paul Stoy[3]

ABSTRACT

The goal of this research, which was the focus of a master's thesis, was to build upon previous investigations of the processes controlling the spatial distribution of snow water equivalent (SWE) in alpine environments. This involved taking a comprehensive look at the widely accepted physiographic variables of: elevation, slope, aspect, solar radiation, and wind exposure, but also avalanche activity, which has been given limited explicit inclusion. The paired basin design adopted in this study, between hypothesized avalanche-prone and avalanche-free basins, has been previously used to correlate avalanche activity with snowmelt runoff. However, it has not been used in an attempt to parse out which variables have the dominant influence on SWE distribution between adjacent areas of very similar physiographic character. While most previous studies have focused on the period of peak SWE to study its distribution, this current research considered the evolution of the controlling variables throughout snowpack development, and subsequent melt-out. A robust dataset of snow depth and SWE measurements were collected January 31 - July 10, 2013 on Cedar Mountain near Big Sky, MT. Physiographic variable values were extracted from a 10 m resolution digital elevation model (DEM) at snow sample points and input as predictors of observed SWE in multiple linear regression (MLR) and binary regression tree (BRT) models to spatially distribute SWE across the study area. Optimal models were selected by various measures of goodness of fit and cross-validation criteria. Calculated R^2 values for MLR models (0.17-0.57) and BRT models (0.33-0.66) were comparable to previous studies indicating a relative level of success in predictive performance. Subsequent analysis of each optimal model's variable selection and predicted SWE distributions revealed differences in the spatial and temporal patterns of this metric between the paired basins, confirming some well-understood processes as well as offering new insights. (KEYWORDS: snow water equivalent, spatial distribution, paired basin, binary regression tree, avalanche)

INTRODUCTION

The combined hydroclimatology and topography of the US Intermountain West lead to snowmelt runoff supplying approximately 67-75% of the annual stream discharge in this region (Cayan, 1996; Serreze et al., 1999; Wise, 2012). The temporal pattern of snowmelt is vital to the functioning of the semi-arid ecosystems in this region, and to the utilitarian needs of the human infrastructure. Operational streamflow forecasting must consider the factors that influence the magnitude and timing of snowmelt runoff in order to harness and allocate water resources appropriately. Consequently, research in snow hydrology has long focused on how to accurately determine the distribution of snow water equivalent (SWE) over landscapes of different scales and degrees of spatial heterogeneity to use as an input for snowmelt runoff models. In alpine watersheds, depending on the scale and climate, the majority of previous investigations have concluded that some combination of the physiographic variables of: elevation, slope, aspect, solar radiation, landcover, and wind shelter/exposure, are dominant in predicting the spatial pattern of SWE (e.g. Elder et al., 1991, 1998; Luce et al., 1998; Balk and Elder, 2000; Winstral et al., 2002; Anderton et al., 2004; Erickson et al., 2005; Harshburger et al., 2010; Clark et al., 2011, Anderson et al., 2014). Some of these studies have mentioned avalanche activity as contributing to the distribution of SWE and subsequent snowmelt runoff, but others have given it explicit consideration as a major predictor (e.g; Sosedov and Seversky, 1965; Iveronova, 1966; Martinec and de Quervain, 1975; de Scally and Gardner, 1988; de Scally, 1996).

This current study builds on previous research by giving equal consideration to all of the aforementioned physiographic variables (i.e. elevation, slope, aspect, solar radiation, and wind exposure) and explicitly considers avalanche activity, to parse out which have the dominant influence on the spatial distribution of SWE through snowpack development, in a paired basin study area in southwest Montana. Analysis was conducted on a dataset

Paper presented Western Snow Conference 2015

[1] Jason Welz and Jordy Hendrikx, Snow and Avalanche Laboratory, Department of Earth Sciences, MSU-Bozeman, jasonwelz@gmail.com, jordy.hendrikx@montana.edu

[2] Stuart Challender, Department of Earth Sciences, MSU-Bozeman, schallender@montana.edu

[3] Paul Stoy, Department of Land Resources and Environmental Science, MSU-Bozeman, paul.stoy@montana.edu

consisting of point measurements of snow depth and SWE acquired during a field campaign in the 2013 water year. Field measurement of snow metrics employed a stratified sampling design adapted from field campaigns with a similar scale and/or goal (Elder et al., 1991; Elder et al., 1998; Winstral et al., 2002; Erickson et al., 2005; Clark et al., 2011). This sampling technique was applied to paired basins with many similar physiographic characteristics, but with sufficient variation to create substantial differences in snowpack distribution, thus warranting comparison. Modeling methodology selection was based on: 1) simplicity, 2) interpretability, 3) appropriateness to data sampling, and 4) performance in similar study designs and scales. Consideration was also given to comparing two modeling techniques with fundamentally different methodologies, resulting in an analysis of the performance between multiple linear regression (linear) and binary regression trees (nonlinear).

STUDY AREA

Research was conducted in paired alpine basins on the east slopes of Cedar Mountain (approximate center: N 45° 14' 3" W 111° 29' 42") in the Madison Range near Big Sky in southwest Montana (Figure 1). The hypothesized, more avalanche-prone basin (Basin A) has an area of 1.38 km^2 rising from 2721 to 3251 m (530 m), with predominantly east to northeast facing terrain forming the headwaters of the South Fork of the West Fork of the Gallatin River. Directly south, the control basin (Basin B) has an area of 1.63 km^2 ranging from 2645 to 3253 m (608 m) with generally east to southeast facing terrain. Average slopes are 24.2° and 22.5° in Basin A and B, respectively, with 31.4% and 26.0% of the area in each basin considered avalanche terrain (slope 30-50°). Both basins are undeveloped and exhibit land cover typical of an alpine environment in this region, with sparse ground cover vegetation covering the majority of the area and riparian shrubs limited to stream channels. Conservative estimation of tree cover utilizing satellite imagery in a GIS, is approximately 7% for Basin A and 19% for Basin B. Tree cover consists entirely of evergreen species.

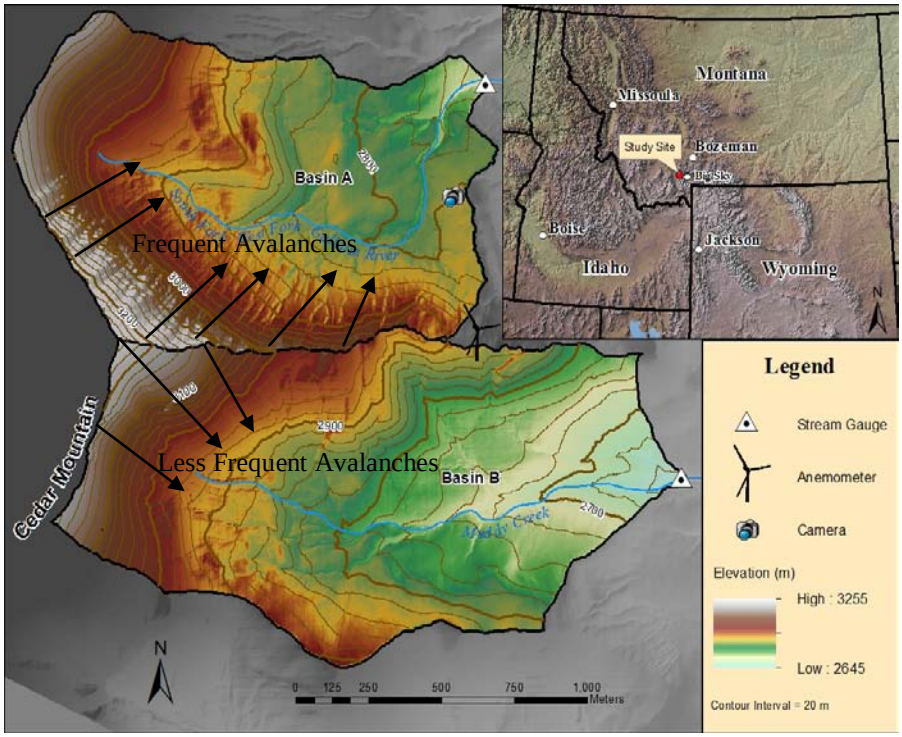

Figure 1. Study site on Cedar Mountain, in the Madison Range near Big Sky, MT

This area of southwest Montana has been generally classified as having an intermountain snow climate (Mock and Birkeland, 2000). However, lying on the northern end of the intermountain zone at high elevation, cold average temperatures result in the snowpack of the Big Sky area to trend more towards a continental regime. The 20-year (1991-2010), October 1 - May 10 average for precipitation (538 mm) and median snow water equivalent (480 mm) from the NRCS Lone Mountain SNOTEL (NRCS, 2014) at 2707 m (approximately 6.5 km from the study site), also indicate this area receives substantially less snow than some intermountain ranges to the south, such as the Tetons (Phillips Bench SNOTEL at 2500 m; precipitation: 729 mm, SWE: 660 mm) and Wasatch (Snowbird SNOTEL at 2942 m; precipitation: 1072 mm, SWE: 1087 mm). This cold and relatively drier climatic pattern has an important influence on the magnitude of snow redistributed by wind, as well as potential avalanche activity that can occur due to persistent weaknesses in the typical stratigraphy of this snowpack. The primary attributes assumed to separate Basin A and B into avalanche-prone and control are their dominant topographic features and distribution of aspect. This applies to the steep, north/northeast facing headwall of Basin A, for which approximately 73% of the slope is 30-50°. This combination of slope and aspect creates more potential for wind loading of snow, causing

frequent sloughing and the occasional release of slab avalanches. In comparison, the east/southeast facing headwall of Basin B has approximately 54% of its slope between 30 and 50°. It is thought to have less potential for avalanche activity due to more wind scour than deposition and a less expansive and contiguous avalanche start zone.

METHODS

Classification of Strata by Physiographic Variables

Snowpack data collection employed a stratified sampling strategy based on the goal of capturing a representative sample from each basin's distribution of physiographic variables. Elevation, slope, aspect, solar radiation, and avalanche zone components were directly modeled from a 1/3 arc second (approximately 10 m cell size) National Elevation Dataset (NED) (*USGS*, 2013) DEM using Spatial Analyst Tools in ESRI ArcGIS. Elevation was reclassified into 10 equal interval (approximately 61 m) strata to span the full range of the study area, 2645-3255 m. In reclassifying slope, its relationship to solar radiation intensity, wind shelter/exposure, and avalanche activity was considered. Hence, lower angle areas, where solar intensity and wind redistribution are less influential, were lumped into a 0-15° strata. Conversely, very steep areas that tend to be largely snow-free due to the more profound effect of these variables along with the constant sloughing of snow, were categorized into 60-90°. For avalanche activity, the second lowest strata, 15-25°, was considered to span the upper limit of runout zones and lower limit of avalanche tracks. Seven 5° strata, spanning 25-60°, were used to classify the remaining terrain, not only to represent the range of over which approximately 98% of all dry-slab avalanches occur (*McClung and Schaerer*, 2006), but to capture the point to hillslope scale topographic features affecting solar intensity/shading and wind redistribution. Aspect was modeled with the Aspect tool in ArcGIS and reclassified into eight, 22.5° degree strata beginning at 0° (north) and running clockwise through 360°. Due to the circular data issue of aspect, it was transformed into a variable of northness and eastness (*Harshburger et al.*, 2010), by taking the cosine and sine of degrees from north, respectively. This yielded surrogate values for aspect between -1 (due south) and +1 (due north) and between -1 (due west) and +1 (due east) that were used in analysis. Area Solar Radiation in ArcMap was used to model the daily cumulative solar radiation in watt hours per square meter (WH/m^2) from November 1, 2012 to May 1, 2013. These values, ranging 115,374-561,342 WH/m^2, were reclassified by natural breaks (Jenks) into ten strata ranging 1-10. While the previously described slope strata indirectly incorporated avalanche activity, a set of slope strata were created to directly sample of the distribution of SWE in the avalanche zone components. This involved reclassifying slope into strata of the typical angle ranges of the avalanche zone components (*McClung and Schaerer*, 2006): (1) runout (<15°), (2) track (15-30°), and (3) start zone (30-50°).

Field Sampling Strategy

Field sampling incorporated aspects of similar studies aimed at sampling SWE (e.g. *Elder et al.*, 1998; *Clark et al.*, 2011) and modifying them to match the scale triplet [spacing, extent, support, after *Bloschl* (1999)] considerations particular to the study area. This strategy evolved while testing and adapting the field sampling methods during accumulation (seven visits: January 31-April 11). The sampling techniques and strategy were solidified by the start of the peak SWE sampling period (six visits: April 30-May 10), and continued during the ablation period (eight visits: June 1-July 10). Because the primary goal of sampling for this study was to capture the spatial distribution of the snowpack metrics during peak SWE, the general location of the transects/points aggregated during the accumulation period was continued during peak SWE sampling period, but modified slightly and supplemented with additional ones to achieve a more representative sample (Figure 2). In order to capture the pattern of the declining snowpack, but limited by the infeasibility of getting more than one sample at all established transects in the allotted timeframe, repeat visits during ablation involved actual measurements at a representative subset of transects. All transects were visited once and repeat visits were made where the snowpack was persistent. Transects where melt-out occurred prior to the end of this survey period were determined to be snow-free from vantage points within the study site. Despite the distinction between sampling periods, the same general methods and scale triplet were maintained during the entire 2013 field campaign.

Field Data Collection and Processing

Snow depth and SWE were measured at points in transects on elevation contours with starting points predetermined in ArcGIS. Transects ranged 150-450 m in extent with points at a15-50 m spacing. Snow depth was measured with a 320 cm avalanche probe at the center of every point, as well as 1 m from the center in each cardinal direction (N, E, S, and W), and the five depths were averaged for analysis. SWE was measured with a Federal snow sampler at a minimum of two, randomly, pre-chosen points along each transect. Average snow density within each transect was back calculated from SWE, then used to interpolate SWE across the entire transect from snow depths.

All field data was recorded in a Trimble Geo XH GPS data dictionary that assigned snow depth and SWE measurements to the sample points during data collection.. Downloaded field data points were differentially corrected. A database of physiographic variables was developed by extracting 10 m DEM cell values for elevation, slope, northness, eastness, solar radiation, and a wind exposure/sheltering variable to the sample points in ArcGIS. This data was imported from ArcGIS and analysed in *R*.

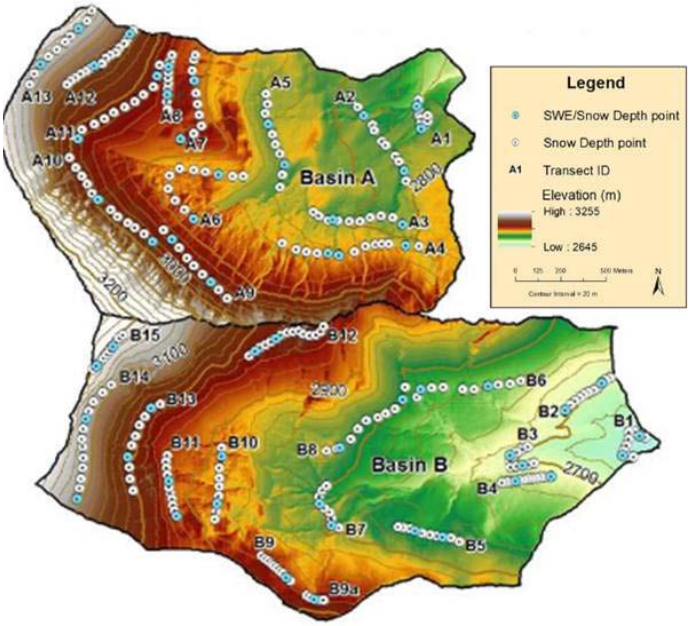

Figure 2. Sampling point and transect distribution for peak SWE.

In order to supplement snowpack measurements with respect to avalanche activity and wind, automated instrumentation was installed prior to sampling (Figure 1). For visual verification of avalanche occurrences, a digital SLR camera was installed facing the northeast headwall of Basin A, and collected photos hourly (08:30-16:30) from December 17 to August 19, 2013. An anemometer (Windlog, RainWise Inc.) was installed at 2808 m on the ridge separating Basins A and B, and recorded average scalar wind speed (m/s) and direction (resolution: 22.5 degrees) at 15 minute intervals from December 17 to March 9, 2013. Water level loggers (HOBO model U20, 0 to 9 m) were installed at the hydrologic pour point of each basin's outlet stream and recorded stage at hourly intervals November 1 to August 21, 2013. Although stream discharge data was collected, correlation with observed and modeled SWE ended up beyond the scope of this research.

Wind Exposure/sheltering Variable

A wind exposure index (WEI), E_b^x, (Lapen and Martz, 1993; Anderton et al., 2004; Anderson et al., 2014) was derived after field sampling in order to quantify the effect of the wind redistribution of snow. This was modeled utilizing directional elevation data to determine the degree of wind exposure or sheltering at sampling points from the equation:

$$E_b^x = z_i - \bar{z}_b^x \quad (1)$$

where z_i is the DEM derived elevation of a given sample point, and $\bar{z}_b^x$ is the average elevation a given filter distance x (m) and bearing b (°) from the DEM pixel (or sample point) of interest.

With the 10 m DEM as input, a series of steps were conducted in ArcMap Tools to model the WEI. The $\bar{z}_b^x$ variable was derived by first determining the correlation length of snow depth data to provide the filter distance (x). This was identified by plotting the snow depth sampling data in a semivariogram in Geostatistical Analyst, yielding a value of 50 m. The upwind bearing direction (b) was determined by the average direction of anemometer records for sustained wind speeds $\geq$ 5 m/s, reflecting the average threshold for transport of dry snow (*McClung and Schaerer,* 2006). One standard deviation was added and subtracted to this value, yielding a bearing wedge of 162-227°. The filter distance (x) and bearing wedge (b) values were used as input, along with the 10 m NED (z), in the Focal Statistics/Spatial Analyst tool to yield a raster of the average elevation of upwind terrain ($\bar{z}_b^x$). This raster was then subtracted from the original 10 m DEM raster (z_i) to yield a raster of E_b^x (WEI). Negative values represent terrain with higher elevation upwind, hence, wind sheltered leading to snow deposition, and positive values indicate terrain with lower elevation upwind, thus wind exposed, leading to snow scouring.

Simple and Multiple Linear Regression

Linear regression modeling was used to analyze the effect of the physiographic (independent/predictor) variables on the distribution of SWE (dependent/response) in each basin during each sampling period. Initially, simple linear regression (SLR) offered a quantification of the effect of each individual variable, as well as the

direction of the relationship with SWE. Subsequent, stepwise multiple linear regression (MLR) then indicated how much the distribution of SWE could be explained by mixed effects between the variables. The maximization of adjusted R^2 was used as the primary measure of model performance with the minimization of residual squared error (RSE) included as an additional check on the trend of model fit. The Akaike Information Criterion (AIC) was targeted as a measure of predictive accuracy versus model complexity cost. Finally, the verification inflation factor (VIF) was used to eliminate models with multicollinearity, or questionable degree of correlation between variables.

The MLR model assumptions of (1) independent observations, (2) randomization (3) linearity, (4) constant variance, (5) normality, and (6) influential outliers were considered in the sampling design and through diagnostic plots to ensure all were reasonably met. Diagnostic review showed linearity in the scatterplots for the WEI and solar radiation and a correlation matrix showed correlation coefficients greater than 0.75 for the pairing of these variables as well as for northness and solar radiation. Thus models with these variable combinations were not included in the results despite having some of the highest R^2 values. Since actual point raster values of each variable were used in analysis, avalanche zone was not included as it was merely a binned classification of slope. Inclusion created a high degree of multicollinearity between slope and avalanche zone, shown in MLR VIF values, indicating that one of these variables had to be removed to avoid redundancy and inaccurate model results.

Binary Regression Trees

Previous investigations into the spatial distribution of SWE in montane catchments (e.g. *Elder et al.*, 1995, 1998; *Balk and Elder*, 2000; *Erxleben et al.*, 2002; *Winstral et al.*, 2002; *Molotch et al.*, 2005) have employed binary regression tree (BRT) methods to distribute this snowpack metric across the landscape. These studies note that this method requires large amounts of data and is therefore more accurate for small catchments, so it was considered appropriate for this current study. The general BRT method developed by *Breiman et al.* (1984) works by "growing" a tree through recursive partitioning (splitting) of dependent (response) variable samples (values), based on independent (predictor) variable values that maximize a decrease in the misclassification rate. This process creates increasingly smaller, more homogenous subsets of the parent, eventually ending with modeled dependent variable values (terminal nodes) with the lowest misclassification probability. This is achieved by an algorithm that performs an optimization decision based on a binary splitting criterion that minimizes the residual sum of squares (RSS) of values within a subset and maximizes this measure between subsets. The sum of the RSS for all terminal nodes equals the total deviance of the model; subtracting this value from the model deviance at the root node yields the model's coefficient of determination (R^2). The analysis for the current study was accomplished in *R* using the *rpart* function involving splits for the dependent variable of SWE based on the data for the physiographic variables.

Overfit trees were pruned in *R* (*rpart*) based on a complexity parameter (cp) which determines the decrease in relative error (of the overall model) necessary to justify the complexity cost of an additional split in the tree (Figure 3). This works by the process of 10-fold cross-validation, in which the original sample is divided into 10 subsets of auxiliary trees by random selection and an algorithm seeks to minimize the misclassification error while holding a different, training subset out for each of 10 possible runs. Because cross-validation involves a randomized process for the initial split on the training subset, each run can produce different estimates of misclassification cost or relative error for the sequence of subsequent splits. To determine a robust estimate of relative error associated with splits, 100 iterations of the cross-validation were run (Winstral et al., 2002; Molotch et al., 2005). To ensure the pruning decisions made in *R* had allowed a tree to grow to optimal size, the '1 SE rule' (Brieman et al., 1984) was manually employed by analyzing plots of the cp and tree size versus the x-val relative error and targeting the smallest tree size where the x-

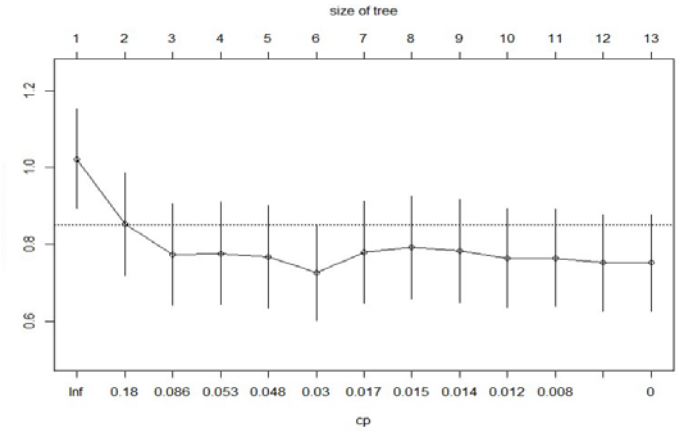

Figure 3. Plot of the complexity parameter (cp) and tree size versus the 10-fold cross-validation error (X-val Relative Error) for each split of the full BRT for Basin B for the peak SWE sampling period. The dashed line indicates the upper limit of 1 standard deviation, hence the optimal tree size is 6 nodes where X-value Relative Error is minimized and the tree still meets the 1 SE rule.

value relative error reaches a minimum that is ± 1 standard error.

MLR and BRT Modeling in a GIS

The linear equations from the optimal MLR models and hierarchical structure of BRT models were utilized as input equations in the ArcMap Raster Calculator to distribute predicted SWE over the study area. The process for MLR involved multiplying rasters, derived from the aforementioned 10 m DEM for each of the physiographic variables, by their MLR coefficients and adding them in the regression equation to yield a modeled spatial distribution of SWE. For the spatial distribution of BRT models, splitting criteria values of the physiographic variables were used in conditional statements to derive SWE values for each raster cell.

RESULTS

Representative Sampling of the Physiographic Variables

The distribution of points sampled in each basin for snow depth and SWE was compared to the distribution of elevation, slope, aspect, solar radiation, and avalanche zone components in each basin in order to assess the representativeness of the sampling design during each data collection period (Table 1). Root mean squared error (RMSE) was used as the measure of fit of the sampling distributions, and RMSE values represent the difference between the distributions of the physiographic variable bins and sampling distributions in percent (%). This was calculated by comparing the percent of raster cells (of total) that fell in each physiographic variable bin to the percent of sampling points that fell into that respective bin. The binning of the physiographic variables substantially reduced their overall variance, thus giving the appearance of more representative sampling than would be possible if each individual raster cell value was considered. The variable of wind exposure/sheltering was not directly analyzed, as it was assumed to be indirectly represented through the sampling of elevation, slope, and aspect.

Of the three periods, the smallest sample was acquired during accumulation with the 1.38 km^2 area of Basin A having 106 snow depth points (76.8 points per km^2) including 14 SWE depths, and the 1.63 km^2 area of Basin B having 63 snow depth points (38.9 points per km^2) including 8 SWE depths. This sampling distribution was least representative of higher elevation zones and steeper slopes. During peak SWE, this was generally overcome with sampling quite proportional to each basin area with 142 snow depths points (102.9 points per km^2) including 27 SWE depths in Basin A and 165 snow depth points (101.9 points per km^2) including 30 SWE depths in Basin B. The representativeness of sampling declined during ablation, mainly due to repeated surveys at several transects, while others only received a single visit. In Basin A, 298 (142 unique points) snow depths including 44 SWE depths were measured and in Basin B, 329 (165 unique points) snow depths including 30 SWE depths. The collective sampling design worked best at representing the variable of aspect during all three periods, with RMSE values less than 4.00. This indicated that, while the sampling distribution was unbalanced between Basin A and B during the accumulation period, it produced a representative sample overall. This also corresponded well to the sampling representativeness of solar radiation during the peak SWE period and ablation periods with RMSE values less than 5.00. The relative representativeness of sampling during the peak SWE and ablation periods is indicated by substantially lower RMSE values in each basin than accumulation.

Table 1. RMSE values for the distribution of the physiographic variables in each basin versus the sampling distribution. RMSE is the difference in percent (%).

	Accumulation		Peak SWE		Ablation	
	Basin A	Basin B	Basin A	Basin B	Basin A	Basin B
Elevation	6.63	8.12	4.58	5.82	5.54	7.43
Slope	7.70	5.66	5.90	3.17	6.53	3.31
Aspect	2.00	3.41	3.97	1.94	2.74	2.16
Solar Radiation	5.26	6.99	4.21	4.51	4.76	4.52
Avalanche Zone	7.59	6.19	5.46	3.81	4.65	3.81

Linear Regression Modeling

For Basin A during accumulation, SLR results showed the top three dominant variables: the WEI, solar radiation, and northness to explain a reasonable proportion of the variance with an R^2 of 0.27, 0.21, and 0.17, respectively. MLR results for Basin A showed the combination of the WEI and eastness to be the best performing model, but with only a minimal increase in adjusted R^2 to 0.28. This was also the most parsimonious model since the inclusion of additional variables showed no increase in R^2 values and increased RSE, AIC, and VIF. For Basin B, eastness was shown by SLR to be dominant followed by the WEI then slope, but the variance explained by the top variables was far less than in Basin A, with R^2 values of 0.15, 0.08, and 0.00. Unlike in Basin A, model performance

increased greatly for Basin B with the addition of independent variables, the best being that with eastness, the WEI, and northness, to yield an R^2 of 0.32. SWE distributed by MLR models yielded a range of 0-1265 mm for a total volume of 680,436.2 m^3 in Basin A and 0-1045 mm for a total volume of 524,251.1 m^3 in Basin B (Table 2).

Table 2. R^2 values, dominant independent variables in order of significance (decreasing p-value) for MLR and in hierarchical order for BRT models, and total modeled SWE volume in each basin for each sampling period.

	MLR			BRT		
	R^2	Independent Variables	Total SWE (m^3)	R^2	Independent Variables	Total SWE (m^3)
Basin A						
Accumulation	0.28	WEI, Eastness	680,436.2	0.38	Solar, WEI	695,570.9
Peak SWE	0.57	WEI, Slope, Eastness	834,958.5	0.66	Solar, WEI, Slope	916,334.2
Ablation	0.22	WEI, Slope, Eastness	263,716.8	0.33	WEI, Northness, Slope	292,504.5
Basin B						
Accumulation	0.32	Eastness, WEI, Northness	524,251.1	0.48	Eastness	531,489.2
Peak SWE	0.33	WEI, Slope Eastness, Elevation	663,421.1	0.53	WEI, Slope Eastness, Elevation	697,387.6
Ablation	0.17	Eastness, Slope, WEI	124,007.6	0.62	Eastness, Solar, Elevation, WEI	131,780.4

During the peak SWE sampling period, the dominant independent variable in Basin A was shown to be solar radiation with an R^2 of 0.53, followed by the WEI and northness with R^2 values of 0.48 and 0.40, respectively (Table 3). Model performance for the peak SWE period showed a modest improvement in Basin A, when combining the WEI with slope and eastness, increasing R^2 to 0.57.. Mostly opposite results were found in Basin B, with WEI being the dominant control shown by an R^2 of 0.23, and with solar radiation and northness not showing nearly as much of the variance explained with R^2 values of 0.12 and 0.09, respectively. The addition of slope with the WEI provided over a 32% increase, for an R^2 of 0.31, indicating the best, two variable model.. Despite the favorable parsimony and relative ease of interpretation of this model, the further addition of eastness and elevation did provide a substantial increase and peak in the R^2 at 0.33. A lowest AIC of 2336.8 and an acceptable VIF of 2.5 also made this model difficult to dismiss despite its four variable complexity. The distribution of SWE for Basin A with the model using the WEI, eastness and slope had a range of 0-2067 mm, while the model for Basin B with the WEI, slope, eastness, and elevation resulted in a SWE range of 0-1243 mm (Figure 4). Modeled total SWE volume was 834,958.5 m^3 in Basin A and 663,421.1 m^3 in Basin B.

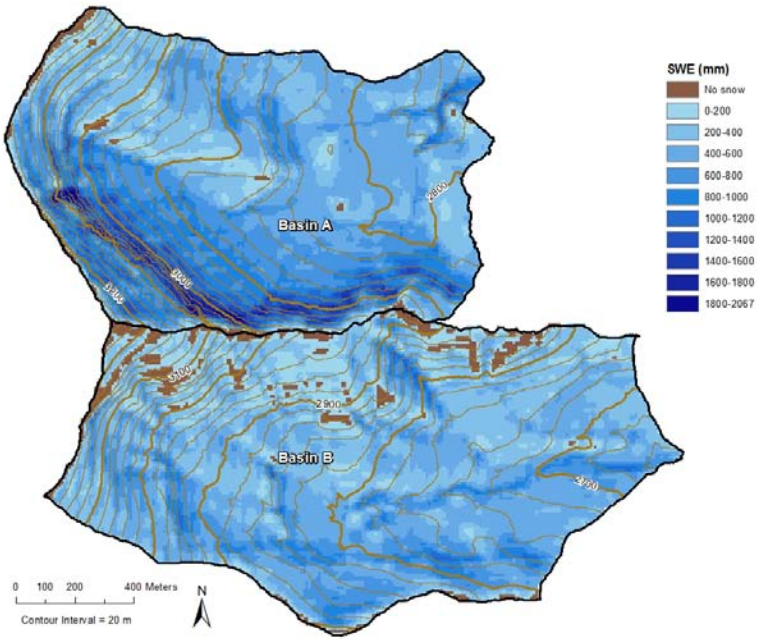

Figure 4. The modeled distribution of SWE for the peak SWE period using MLR models: Basin A: *SWE ~ 296.78 + (-93.02)*WEI + (148.85)*Eastness + (7.99)* Slope*; Basin B: *SWE ~ 1410.72 + (-83.05)*WEI + (11.52)*Slope + (180.03)*Eastness + (-0.43)*Elevation.*

Continuing with the pattern of peak SWE, solar radiation, followed by the WEI and northness, once again

proved to be the principal variables controlling SWE in Basin A during ablation with SLR R^2 of 0.17, 0.17, and 0.11, respectively. Despite its low R^2 of 0.00, slope, and eastness, not shown to be significant ($\alpha = 0.05$) in SLR, proved to have the best mixed effect in MLR with the WEI, producing an R^2 of 0.22. The SLR models for Basin B actually reversed compared to the previous sampling periods to show eastness, slope, and elevation as the most influential with R^2 values of only 0.10, 0.06, and 0.04. The best performing and most parsimonious MLR model combined eastness, slope, and the WEI for an R^2 of 0.17. The distribution of SWE modeled by MLR for Basin A with the WEI, slope, and eastness yielded a range of 0-1029 mm, for a total volume of 263,716.8 m^3, while the model for Basin B with eastness, slope, and the WEI resulted in a SWE range of 0-631 mm, for a total modeled volume of 124,007.6 m^3 in (Table 2).

Binary Regression Tree Modeling

The root node of the BRT, or variable modeled as most influential in predicting SWE in Basin A during the accumulation period, was solar radiation. The initial split from the root node suggested that locations with the lowest SWE depths (terminal node = 191 mm) were solely controlled by solar radiation if incoming levels exceeded the splitting criterion of 453,300 W/m^2. Below this level, wind became an important factor, and areas with less negative WEI values (more wind exposed) were limited to a moderate level of SWE (terminal node =454 mm), while those with more strongly negative WEI values (more wind sheltered) held the deepest SWE (terminal node = 612 mm). This tree partitioned 15.1% of the sample points (n = 16) to the lowest SWE, 26.4% (n = 28) to midlevel SWE, and 58.5% (n = 62) to the highest SWE. The Map Algebra/Raster Calculator tool in ArcGIS was utilized to gain a spatial distribution of SWE and estimate a total SWE volume of 695,570.9 m^3 (Table 1). The BRT for Basin B pruned down to a very simple tree with one split on the root node of eastness with a criterion value of 0.879 leading to modeled values of 259 and 645 mm of SWE in the terminal nodes. This partitioned 69.8% of the sample points (n = 44) to the 259 mm of modeled SWE, 30.2% (n = 19) to 645 mm. The spatial distribution of SWE totaled a volume of 531,489.2 m^3, 23.5% less than in Basin A despite Basin B being 15.2% larger in area (Table 2).

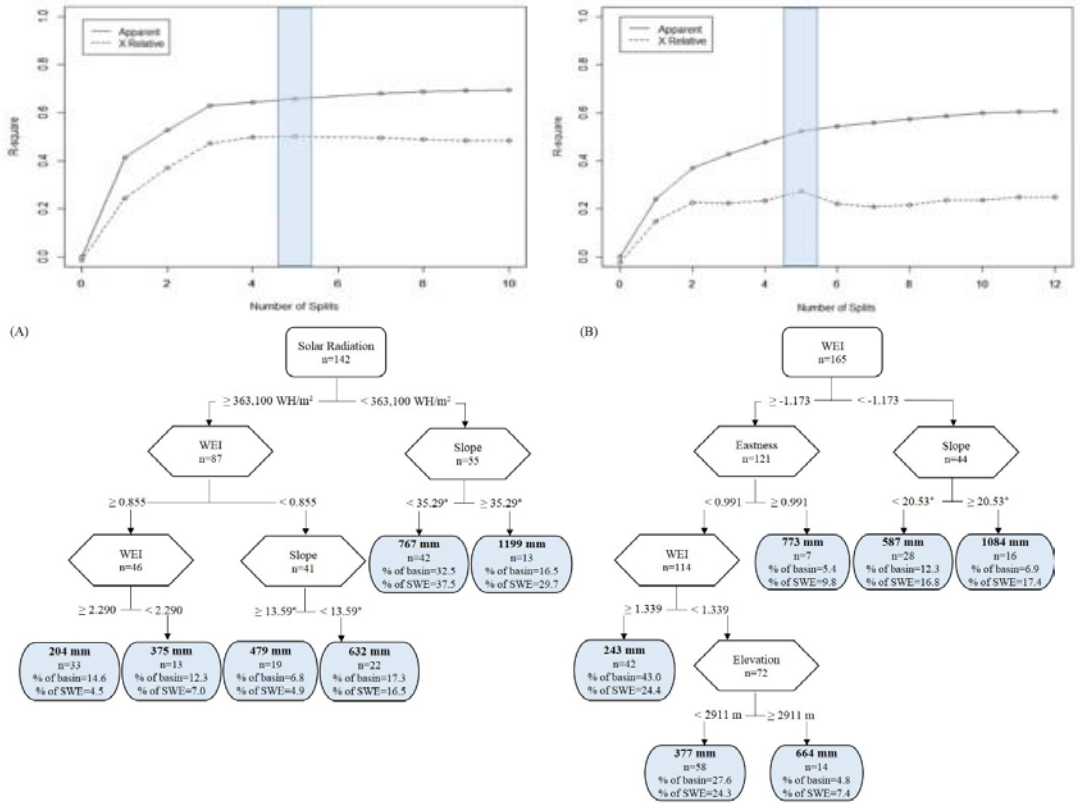

Figure 5. Pruned binary regression trees for Basin A (A) and Basin B(B) for peak SWE with corresponding plots of R-square (apparent and relative to cross-validation error) versus number of splits to verify optimal tree size (highlighted in blue)

For peak SWE, the BRT for Basin A (Figure 5) grew from a root node of solar radiation, with the WEI and slope offering further predictive value by splitting into two different tiers of daughter nodes. These subsequently grew a total of 6 terminal nodes for modeled SWE with a range of 204-1199 mm, explaining 66% of the variance. The spatial distribution displayed a fairly distinct dichotomy in the basin with the southern half (northeast facing zone) harboring more than 60% of the 916,334 m^3 of modeled SWE (Figure 6). The WEI was shown to be the dominant variable in Basin B, with a root node growing into recursive splits on eastness and slope and then the WEI and elevation. The final 6 node tree explained 52% of the variance in SWE with a range of 243-1084 mm. The spatial distribution of SWE was a bit more of a mosaic than that in Basin A. This did, however, reveal a pattern of the deepest deposits being predominantly in the southern half of the basin, particularly in north and east aspects at mid to high elevation. These zones of deep SWE only covered less than 20% of the basin, reflecting a total modeled basin SWE of 697,387 m^3 that was 24% less than in Basin A.

Transitioning from peak SWE into the ablation period, the BRT model for Basin A shifted from one based on a root node of solar radiation to the WEI. The WEI was solely responsible for modeling the zones of highest SWE, while further splits on northness and slope determined low to midlevel SWE values in explaining 33% of the variance. With this sampling period spanning into early July, 80.9% of the basin was modeled with the lower values (48 and 173 mm) of SWE; however, the two higher values of SWE (466 and 804 mm) that covered only 19.1 % of the basin, accounted for 66.3 % of the remaining 292,504 m^3 (Table 2) of SWE. The BRT for Basin B grew from a root node of eastness with recursive splits on solar radiation, elevation, and the WEI resulting in a tree of 5 terminal nodes that explained 62% of the variance in SWE. The initial split on eastness determined that, at this point, 80.8% of the basin area that is only slightly off of this aspect was close to melt-out with only 35 mm of modeled SWE. This accounted for 34.9 % of the total volume of 131,780.4 m^3. On the other end of the spectrum, 1.3 % of the basin area with an aspect very close to due east and low solar input was modeled with 1606 mm of SWE, maintaining 26.2% of the total volume. Further splits occurred first, on a value (2926 m) very close to the midpoint of the elevation range and finally on the WEI which divided zones of 65, 239 and 1117 mm, overall leading to a spatial distribution marked by abrupt changes in SWE depths.

DISCUSSION

Representative Sampling

The sampling distributions were markedly different between the accumulation, peak SWE, and ablation phases of snowpack development. Due to time, weather, and avalanche based safety constraints, the smallest number of samples were obtained during accumulation. Upper elevation zones were undersampled, not only due to heightened avalanche danger, but significant cliff areas that were mainly inaccessible. Previous studies (e.g. Elder et al., 1991, Balk and Elder, 2000, Winstral et al., 2002, Erickson et al., 2005) have noted similar limitations on representative sampling even during the peak SWE period when snowpack conditions are normally more stable. Because peak SWE was the snowpack phase of focus, the study basins were sampled intensively during an 11 day time span, yielding the most consistent and evenly distributed dataset. With a melt freeze cycle occurring during much of this period, avalanche terrain at nearly all elevations was able to be safely sampled; however, some very steep zones, particularly

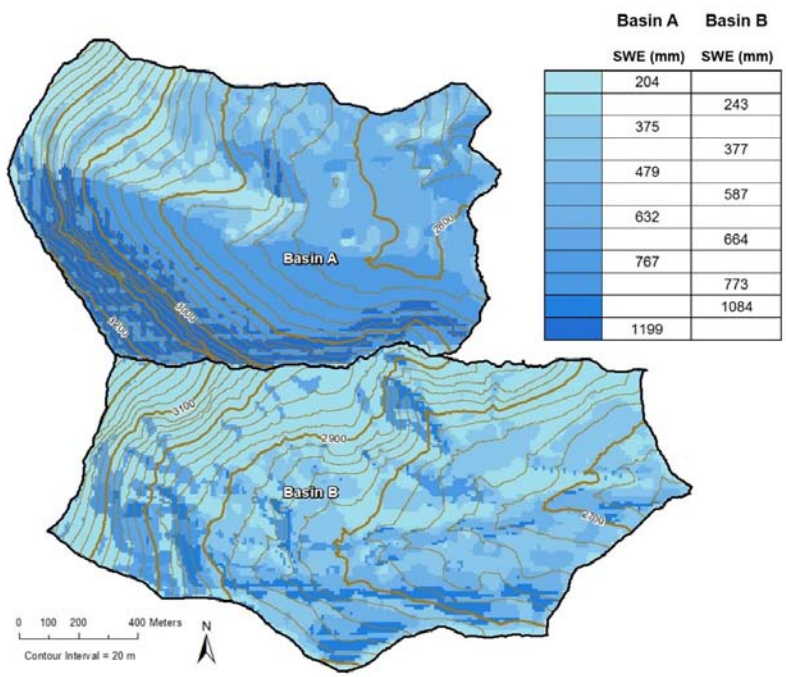

Basin A SWE (mm)	Basin B SWE (mm)
204	
	243
375	
	377
479	
	587
632	
	664
767	
	773
	1084
1199	

the northeast headwall of Basin A, were still inaccessible. The lack of sampling in the largest contiguous avalanche start zone and source of continual sloughing, limited correlation of subsequent snow distributions to avalanche activity in this zone and below. The oblique, orthorectified photography technique utilized by Kerr et al. (2013) to determine the spatial distribution of SWE in avalanche terrain would be a possible solution to this problem. Despite the largest sample size being acquired during the ablation period, its representativeness suffered from repeat data observations in persistent snowpack areas, as opposed to patchy or snow-free areas, in the interest of possible correlations to increased deposition from avalanche activity and wind redistribution.

As previously mentioned, consideration of the scale triplet, as defined by Bloschl (1999), is crucial to a sampling and modeling design. The fundamental issue with choosing the appropriate scale triplet is that the process scale (correlation length) in an unstudied area is unknown. In their study of sampling scale effects on environmental monitoring, Skoien and Bloschl (2006) stated as rules of thumb: 1) extent should be substantially larger than the correlation length, 2) spacing should be smaller than the correlation length, and 3) support depends on the statistic of interest, but variances are significantly biased and underestimated once support is greater than one third of the correlation length. The previous studies with similar spatial variability in snow depth have used spacings of 5-100 m and extents of 1-93 km^2 (Clark et al., 2011). Thus, this study employed a 15-50 m spacing to capture the point to smaller hillslope scale variability, a 150-450 m transect extent to capture the larger hillslope to watershed scale, within transect, variability, and up to a 1.8 km extent between transects to capture the greater watershed scale variability in snow depth. Support (modeling) was provided at a 10 m scale by the DEM utilized to model the physiographic variables. Post field measurement, the correlation length of snow depth from observed values was estimated to be 55 m. Hence, it is believed that spacing, extent, and support were appropriately chosen for this study given the rules of thumb suggested by Skoien and Bloschl (2006). Erxleben et al. (2002) expressed that their study with a 5-25 m spacing and 30 m DEM support may have resulted in a mismatch of scales for the dependent and independent variables, thus leading to low explained variance by subsequent modeling. This current study limited this scale issue through a better pairing of spacing and support, and R^2 for models, especially during the peak SWE sampling period, are on par with those of other studies.

Accumulation Period

Wind was expected to be a dominant variable during this snowpack phase, as colder air temperatures and hence, lower snow density in the winter allow for maximum snow redistribution. This was shown by SLR analysis to be true in Basin A, with the greatest amount of the variance in SWE explained by the WEI. It was unexpected to see solar radiation not far behind in predictive power, as it seems that the average solar zenith angle and daylight hours at the 45° latitude zone during this period would limit the influence of solar radiation, as well as northness. However, Anderton et al. (2004) noted that earlier in the season, differences in solar input are more profound between northerly and southerly aspects in complex topography due to the low solar zenith angle, whereas solar radiation becomes more uniformly distributed as the solar zenith angle becomes larger approaching the summer equinox. Considering that sampling occurred at some transects through April 11, it becomes more logical that solar radiation would have a strong influence on the overall sample and thus, derived models. Additional variables in MLR did not offer much improvement over SLR with the WEI.

Overall, the SLR models for Basin B had less than half the predictive power than that for Basin A. This disparity is possibly due to the much smaller sample size collected in Basin B during this period compared to Basin A, leading to greater variability in the data. This may also explain why eastness came out with nearly twice the predictive power than the WEI in Basin B, as the two due east facing transects (B10a and B13a) accounted for 26 of the 63 total points sampled during this period, and they also harbored the deepest snow. Despite having nearly half the predictive power, the addition of the WEI to eastness produced substantially better performance in an MLR model than the two variables individually. It also explained more of the variance in SWE than the same model in Basin A. This is consistent with the exposure of the majority of Basin B to wind with a far less prominent topographic barrier to the south/southwesterly flow than the northeast headwall creates in Basin A.

The BRT models for this period generally reflected the dominant variables in SLR analysis, but there were some clear differences from the MLR models. This was seen in the BRT model for Basin A that stemmed from solar radiation and the WEI, while the MLR model, limited by a multicollinearity violation in combining these variables, found the highest R^2 with the WEI plus eastness. Consequently, the BRT was able to explain 38% of the variance while the MLR only explained 28%. However, the BRT was limited to 3 nodes for a range of 191-621 mm of SWE while the MLR was seemingly more accurate in capturing the observed range 0-878 mm with 0-1265 mm. These

issues seem to correspond to the MLR and BRT models for Basin B as well. Again, the SLR and BRT results generally agreed, with eastness being the dominant variable. Overall, the MLR models appeared to capture far more of the point to hillslope scale variability than the BRT models that were basically comprised of three and two distinct zones of accumulation for Basins A and B, respectively. These BRT models had substantially fewer nodes than previous studies (e.g. Elder et al., 1998; Balk and Elder, 2000; Erxleben et al., 2002; Winstral et al., 2002; Anderton et al., 2004; Molotch et al., 2005) that found trees with 5 to 25 nodes to be optimal. This is likely due to the rather small number of observations and general lack of representativeness of the sampling that occurred during accumulation. This produced a higher degree of data heterogeneity (than in the peak SWE sampling period), and as noted by *Elder et al.* (1995), outliers of abnormally deep snow deposits and snow-free areas decreased the potential for further partitioning into nodes of increasing homogeneity. However, while the BRTs were perhaps overly simplistic and did not manage to explain some of the variance, MLR likely overpredicted detail in the distribution of SWE that the data does not support. Although the MLR and BRT models demonstrated some obvious contrasts in variable structure and spatial distribution of SWE, the difference in estimated total volume of SWE was only 2.2% for Basin A and 1.4% for Basin B (Table 2).

Peak SWE Period

A working hypothesis was that solar radiation overcomes the influence of wind on the snowpack by the peak SWE period. This is primarily due to the more direct solar zenith angle and long daylight hours providing increased energy input, as well as the higher average snow density limiting wind transport. SLR analysis supported this hypothesis for Basin A. However, the WEI remained closely influential in Basin A and came out as the dominant variable for Basin B in SLR. The potential for the single variable dominance of WEI in Basin B was considered while field sampling and visually observing substantial wind transport of snow to transects B11 and B13. These transects spanned a shallow concave bowl on the lee of a very broad northwest to southeast trending ridge with no substantial topographic barriers to the Madison Valley. Wind deposition was further verified by the highest measured SWE values in Basin B at these transects. In MLR analysis, the WEI was shown to be dominant in both basins. This was not surprising, as wind had been involved in distributing snow throughout accumulation and had somewhat predetermined the pattern of SWE by early May. Northness was close behind these two in its predictive value, as it is a reflection of both the WEI, given the prevailing southerly winds, and solar radiation as a function of aspect. Unlike during accumulation, this variable was shown to have the logical, positive relationship with SWE, pointing towards the far more representative sample collected during peak SWE. Elevation showed nearly the same R^2 in Basin A as during the accumulation period, suggesting that this variable is somewhat responsible for the distribution of SWE due to orographics and lapse rate, but in reality, this is probably limited by the 600 meters of vertical relief in the study area. The increasing redistribution of snow by wind with elevation, compounded by solar radiation, further limits the explicit effect of elevation and explains why transects A11, A12, and A13, despite their high elevation, are where some of the lowest SWE values were consistently measured.

The timing consistency and relative representativeness of sampling during the peak SWE period produced BRT models that were comparatively successful with regard to previous studies that were conducted during this time period with similarly intensive surveys. The trees, optimally pruned to 6 nodes for prediction in each basin, were relatively small, yet the explained variance (66% in Basin A and 53% in Basin B) was either on par with, or greater than previous studies with similar or greater complexity in their models. Elder et al. (1998) developed trees of 13 to 25 terminal nodes that explained 60-70% of the variance for a hypothetically more difficult distribution due to the substantially larger study area. However, these comparatively larger trees were proportional to the larger dataset (709 sample points) acquired for that study. In a more similarly sized basin of 6.9 km^2, Balk and Elder (2000) explained 54% and 65% of the variance in SWE, nearly equal to the current study, with 18 nodes each for datasets of 197 and 173 snow depth samples, respectively. The similarly sized trees of 5 and 7 nodes (average n = 328) developed by Molotch et al. (2005) explained substantially less variance at 31% and 39%, respectively, but in a larger basin (19.1 km^2). The use of R^2 values as a comparison criterion of model success between studies should include the caveat that these values are not necessarily directly comparable due to the different attributes of the study areas, sampling design, water years, climatology, etc. That being considered, the model performance for the peak SWE period of this current study is encouraging with regard to previous studies. This is especially true considering that within the cross-validation process of pruning, there is a range in the optimal tree size in which the model user has the freedom to decide which is most appropriate given an intimate knowledge of the processes at work in the study area. Thus, the models for the current study appear to exhibit a high level of predictive value given their relative parsimony in comparison to previous studies.

Ablation period

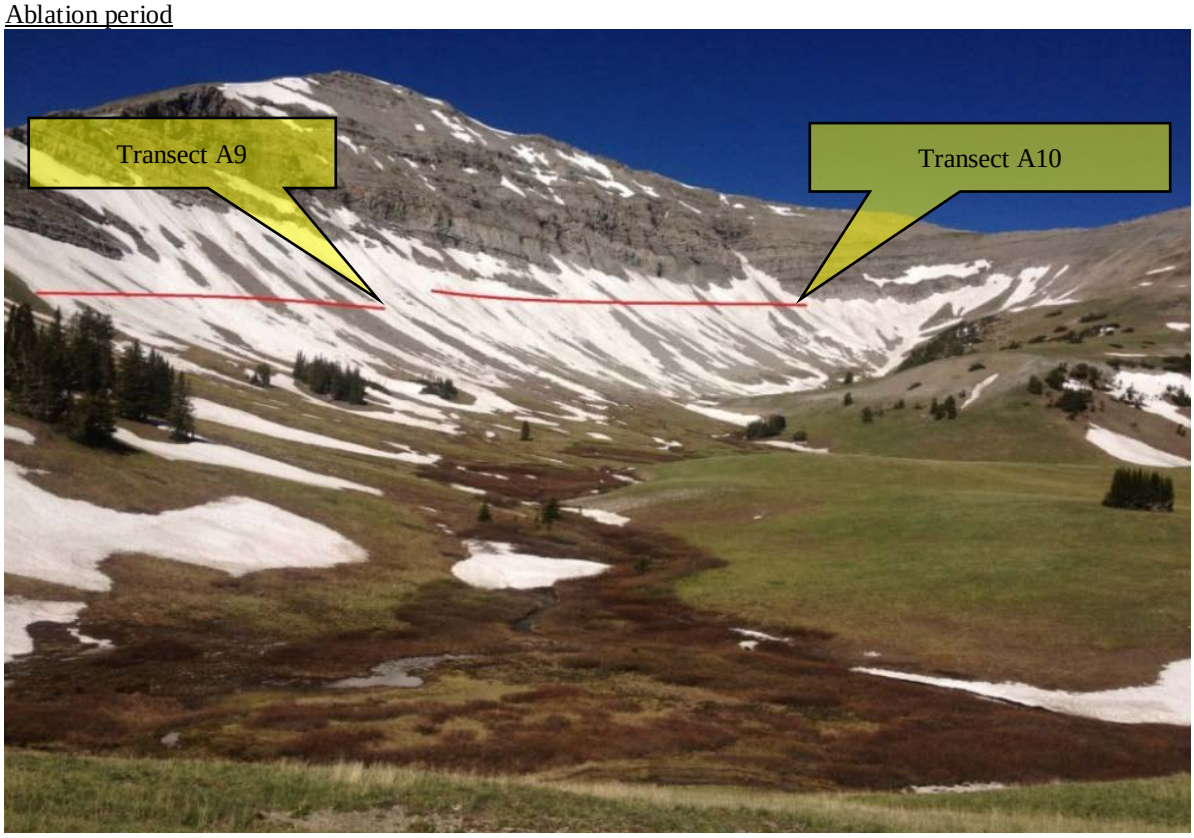

Figure 7. View of Basin A on June 27, 2013 looking west at the headwall (left), and persistent snowpack in Transects A9 and A10.

The SLR results in Basin A continued the pattern from the peak SWE period with solar radiation, followed by the WEI and northness, once again proving to be the principal variables controlling SWE during ablation. This was consistent with our hypothesis, given that solar radiation, and inversely, northness, is assumed to become increasingly important in the energy budget of the snowpack as the melt season progresses. However, a combination of the WEI with slope and eastness resulted in the best performing MLR model despite the latter two variables very little predictive value by themselves. The WEI showing dominance and solar radiation being eliminated in the MLR models is once again due to multicollinearity prohibiting these two variables together in a model. Despite this limitation, the best selected model generally reflected the pattern of melt-out observed during this period while sampling in Basin A (Figure 7), in that, the wind sheltered zones (negative WEI values; coefficient = -48.57), particularly below the north/northeast headwall, with greater slope angles (coefficient = 6.304) with a northeast aspect (eastness values closer to 1; coefficient = 63.905) maintained the deepest snow (Transects A9 and A10). On the other hand, those areas with a more southeast aspect had mainly been scoured by wind, compounded by increased solar input, and were mainly snow-free. Unfortunately, this model was unable to capture the processes of continual sloughing and occasional slab avalanche activity that are presumed to have been the dominant processes at work to leave the upper elevation, northeast facing portion of the headwall in Basin A snow-free by this point. However, that is simply due to the absence of sampling in this zone because of terrain and safety limitations. Nevertheless, it is possible that the persistent snowpack below this headwall is more due to the slope/avalanche activity and solar radiation/northness variables than the combination of the WEI (negative values; wind shelter), slope, and eastness. While sampling and modeling data cannot directly substantiate this inference, many wet slides were observed pouring off the headwall during periods of intense solar heating and debris was photo documented (Figure 8).

Figure 8. View southeast at the headwall of Basin A on June 3, 2013 (left) showing multiple point release wet avalanches, and a close-up of one of the debris piles (right) that averaged approximately 1.5 m in depth.

The performance of the optimally pruned BRT model for Basin A declined substantially for the ablation period, while it improved for Basin B. Similar to the accumulation period, this is suspected to be rooted in the inconsistency and lack of representativeness in sampling during ablation. With 298 observations in Basin A and 329 in Basin B, the ablation period was not data limited. This was evidenced by fully grown tree sizes of 21 nodes for Basin A and 23 nodes for Basin, and it showed that maximum tree size throughout the three sampling period was roughly proportional to the number of observations. However, the high degree of heterogeneity within the ablation dataset between snow-free areas and those harboring unusually deep snow deposits limited the ability of trees to accurately predict this variability, increasing the probability of misclassification. Thus, optimally pruned trees were limited to 4 nodes in Basin A and 5 nodes in Basin B, which explained 33.3% and 62.3% of the variance in SWE, respectively. It is unclear why model performance for Basin B with only 1 additional node was so much better than for Basin A. A possible explanation is that transect locations in Basin B (Figure 6) just happened to be ideal at this point for predicting the distribution of SWE through the tree hierarchy of eastness, solar radiation, elevation, and the WEI. In other words, sampling points either had little or no snow or very deep snow, with few mid-level SWE depths. Thus, the optimal tree could partition this data into fairly homogenous subsets without increasing cross-validation relative error. On the other hand, the sample points in Basin A displayed a higher degree of heterogeneity between snow-free, low, midlevel, and high SWE depths, thereby making it increasingly difficult for trees to partition observations in increasingly homogenous subsets without increasing the probability of misclassification. Due to these potential issues with the sample representativeness of the declining snow pattern, as well as being during a different phase of snowpack development, a direct comparison of the explained variance between BRT models for this and previous studies does not seem appropriate. Despite these issues, the variance explained by the BRT model for Basin A is still acceptable and the fit for Basin B is actually quite good.

CONCLUSIONS

The goal of this study was a comprehensive analysis of the physiographic variables controlling snowpack processes in an alpine environment in order to accurately distribute SWE from point measurements. Previous studies have indicated that correlations of SWE distribution with physiographic variables is very complex and an understanding of these interactions is difficult to develop from a short survey period, such as during the peak SWE snowpack phase, that offers only a small snapshot in time. Hence, this study expanded the investigation through the entire evolution of the snowpack. Since there have also been indications in previous work that the correlations lengths of snow metrics can vary on a number of scales between adjacent basins of similar physiographic character, a paired basin study was employed to parse out these effects. This design also allowed for a comparison of suspected avalanche-prone and non avalanche-prone basins, as treatment and control groups, to explicitly examine the influence of avalanche activity on the distribution SWE, which has not been completely addressed by previous

studies. Finally, a comparison of linear and nonlinear modeling methodologies, both with demonstrated success in different applications of distributing SWE, was conducted to determine which offer more accurate prediction of SWE at the selected scale and environment of the study site.

Field measurement of snow depth and SWE, while employing the same technique, resulted in substantially different samples between the periods of accumulation, peak SWE, and ablation due to weather, safety, and time constraints as well as different considerations on how to gain a representative sample of the evolving snowpack pattern for a given period. This lead to very different models in terms of structure (dominant variables) and performance. The most consistent and representative sample was acquired during the peak SWE period. Sampling during accumulation suffered from limited observations leading to imbalance between basins, while imbalance occurred between in-basin transects during ablation despite having the largest sample size by two fold. These sampling distributions lead to peak SWE models demonstrating the best performance in explaining the most variance in the distribution of SWE. A notable exception is the BRT model for Basin B during ablation, which not only explained an impressive 62% of the variance but very accurately predicted the pattern of melt-out and persistent snow deposits that were observed during field visits. It was clear from snowpack observations, model structures and predicted SWE distributions that the accumulation and peak SWE periods had a profound influence on these elements during ablation. Hence, the pattern of snowpack melt-out was somewhat predetermined, despite a logical shift in dominance of variables controlling this process. Despite the variation between MLR and BRT models with regard to the dominant variables used, the spatial distribution of SWE and relative performance, the estimated total volumes of SWE were very similar between these methodologies (within 1 to 11%). The results of this study are consistent with those of previous studies, with BRT models offering more accurate prediction of distributed SWE compared with other methodologies when a sufficiently large dataset was available. Nevertheless, MLR, as well as BRT models in this study, left a substantial amount of the variance unexplained, especially during the accumulation and ablation periods. This can be mainly attributed to sample size and representativeness.

While the sampling strategy and modeling methodologies of this study did not allow for a statistically defensible indication of avalanche activity having a significant effect on the distribution of SWE alongside the other physiographic variables, qualitative evidence of this potential was obvious in correlations between visual observation and modeling distributions for Basin A.

REFERENCES

Anderson, B. T., J. P. McNamara, H.-P. Marshall, and A. N. Flores. 2014. Insights into the physical processes controlling correlations between snowdistribution and terrain properties, *Water Resour. Res.*, *50*, 1-19.

Anderton, S. P., S.M. White, and B. Alvera. 2004. Evaluation of spatial variability in snow water equivalent for a high mountain catchment, *Hydrol. Processes*, *18*, 435–453.

Balk, B. and K. Elder. 2000. Combining binary decision tree and geostatistical methods to estimate snow distribution in a mountain watershed, *Water Resour. Res.*, *36*, 13-26.

Blöschl, G. 1999. Scaling issues in snow hydrology monitoring, *Hydrol. Processes*, *13*, 2149-2175.

Breiman, L., J. H. Friedman, R. A. Olshen, and C. J. Stone. 1984. *Classification and Regression Trees*, Boca Raton, FL: Chapman and Hall/CRC.

Cayan, D.R. 1996. Interannual climate variability and snowpack in the western United States, *J. of Climate*, *9*, 928-948.

Clark, M.P., J. Hendrikx, A.G. Slater, D. Kavetski, B. Anderson, N.J. Cullen, T. Kerr, E.Ö. Hreinsson, and R.A. Woods. 2011. Representing the spatial variability of snow water equivalence and land surface models: a review, *Water Resour. Res.*, *47*, W07539 1-23.

de Scally, F. A. and J. S. Gardner. 1988. The hydrological importance of avalanche snow, Kaghan Valley, Himalaya Mountains, Pakistan, *International Snow Science Workshop, Whistler, B.C., Oct. 11-15, 1988.*

de Scally, F.A. 1996. Avalanche snow melting and summer streamflow differences between high–elevation basins, Cascade Mountains, British Columbia, Canada, *Arctic and Alpine Res.*, *28*(1), 25–34.

Elder, K., J. Dozier, and J. Michaelsen. 1991. Snow Accumulation Distribution in an Alpine Watershed, *Water Resour. Res.*, *27*(7), 1541-1552.

Elder, K., J. Michaelsen and J. Dozier. 1995. 'Small basin modeling of snow water equivalent using binary regression tree methods' in *Biogeochemistry of Seasonally Snow-Covered Areas*, IAHS-AIHS and IUGG XXI General Assembly, Boulder, Colorado, July, 1995. Internat. Assoc. of Hydrol. Sci., Wallingford, 129-139.

Elder, K., W. Rosenthal, and R.E. Davis. 1998. Estimating the spatial distribution of snow water equivalence in a montane watershed, *Hydrol. Processes, 12*, 1793 – 1808.

Erickson, T.A., M.W. Williams, and A. Winstral. 2005. Persistence of topographic controls on the spatial distribution of snow in rugged mountain terrain, Colorado, United States, *Water Resour. Res.*, *41*, w04014 1-17.

Erxleben, J., K. Elder, and R. Davis. 2002. Comparison of spatial interpolation methods for estimating snow distribution in the Colorado Rocky Mountains, *Hydrol. Processes, 16*, 3627-3649.

Harshburger, B.J., K.S. Humes, V.P. Walden, T.R. Blandford, B.C. Moore and R.J. Dezzani. 2010. Spatial interpolation of snow water equivalency using surface observations and remotely sensed images of snow-covered area, *Hydrol. Processes, 24*, 1285–1295.

Iveronova, M. I. 1966. The hydrological role of avalanches, in *Proceedings, International Symposium on Scientific Aspects of Snow and Ice Avalanches, Davos, April, 1965*, Internat. Assoc. of Sci. Hydrol. Publication, 69, 73-77.

Kerr, T., M. Clark, J. Hendrikx, and B. Anderson. 2013. Snow distribution in a steep mid-latitude alpine catchment, *Adv. Water Resour.*, *55*(0), 17–24.

Lapen, D.R. and L.W. Martz. 1993. The measurement of two simple topographic indices of wind sheltering-exposure from raster digital elevation models. *Comput. Geosci.*, *19*(6): 769–779.

Luce, C., D. Tarboton, and K. Cooley. 1998. The influence of the spatial distribution of snow on basin-averaged snowmelt, *Hydrol. Processes, 12*, 1671–1683.

Martinec, J. and M. R. de Quervain. 1975. The effect of snow displacement by avalanches on snowmelt and runoff, *Proceedings, Snow and Ice Symposium, Moscow, 1971*, Internat. Assoc. of Sci. Hydrol. Publication, 104, 364-377.

McClung, D. and P. Schaerer. 2006. The Avalanche Handbook. Seattle, WA: The Mountaineers.

Mock, C.J. and K.W. Birkeland. 2000. Snow Avalanche Climatology of the Western United States Mountain Ranges, *Bull. Amer. Meteorol. Soc.*, *81*, 2367–2392.

Molotch, N.P., M.T. Colee, R.C. Bales, and J. Dozier. 2005. Estimating the spatial distribution of snow water equivalent in an alpine basin using binary regression tree models: the impact of digital elevation data and independent variable selection, *Hydrological Processes*, *19*, 1459-1479.

Natural Resource Conservation Service (NRCS). 2013. "Snow Telemetry (SNOTEL) and Snow Course Data and Product", at http://www.wcc.nrcs.usda.gov/snow/. Site visted April 4, 2013.

Serreze, M.C., M.P Clark, R.L. Armstrong, D.A. McGinnis, and R.S. Pulwarty. 1999. Characteristics of the western United States snowpack from snowpack telemetry (SNOTEL) data, *Water Resour Res.*, *35*, 2145 – 2160.

Sosedov, I. S. and I.V. Seversky. 1965. On hydrological role of snow avalanches in the northern slope of the Zailiysky Alatau, *Proceedings, International Symposium on Scientific Aspects of Snow and Ice Avalanches, Davos, April, 1965*, Internat. Assoc. of Sci. Hydrol. Publication, 69, 78-85.

Skoien, J.O. and G. Bloschl. 2006. Sampling Scale Effects in Random Fields and Implications of Environmental Monitoring, *Environ. Monit. Assess.*, *114*, 521-552.

United States Geological Survey (USGS). 2013. "NED Spatial Metadata", http://ned.usgs.gov/downloads.html. Site visited January 16, 2013.

Winstral, A., K. Elder, and R.E. Davis. 2002. Spatial snow modeling of wind- redistributed snow using terrain–based parameters, *J. of Hydrometeorol.*, 3:524–538.

Wise, E. K. 2012. Hydroclimatology of the US Intermountain West, *Progresss in Phys. Geog.*, 1-22.